Far-infrared intersubband photodetectors based on double-step III-nitride quantum wells

Faisal F. Sudradjat, Wei Zhang, Jeffrey Woodward, Habibe Durmaz, Theodore D. Moustakas et al.

Citation: Appl. Phys. Lett. **100**, 241113 (2012); doi: 10.1063/1.4729470
View online: http://dx.doi.org/10.1063/1.4729470
View Table of Contents: http://apl.aip.org/resource/1/APPLAB/v100/i24
Published by the American Institute of Physics.

APPLIED PHYSICS LETTERS **100**, 241113 (2012)

Far-infrared intersubband photodetectors based on double-step III-nitride quantum wells

Faisal F. Sudradjat, Wei Zhang, Jeffrey Woodward, Habibe Durmaz, Theodore D. Moustakas, and Roberto Paiella[a)]

Department of Electrical and Computer Engineering and Photonics Center, Boston University, 8 Saint Mary's Street, Boston, Massachusetts 02215, USA

(Received 3 May 2012; accepted 29 May 2012; published online 14 June 2012)

Far-infrared photoconductive detectors based on intersubband transitions in III-nitride semiconductor quantum wells are demonstrated. The device active material is based on a double-step quantum-well design, where two different (Al)GaN compositions are used both in the wells and in the barriers. With this approach, one can create a virtually flat multiple-quantum-well potential energy profile, where the deleterious effects of the intrinsic spontaneous and piezoelectric fields of nitride heterostructures are almost completely eliminated. Photocurrent spectra centered at a wavelength of 23 μm (13 THz frequency) are resolved up to 50 K, with responsivity of approximately 7 mA/W.
 [http://dx.doi.org/10.1063/1.4729470]

In recent years, numerous applications of terahertz (THz) [and more generally far-infrared (FIR)] radiation have emerged, including biomedical sensing, explosive and drug detection, security screening, industrial process control, and spectroscopic imaging for astronomy and space physics. Intersubband (ISB) transitions in semiconductor quantum wells (QWs) provide a leading optoelectronic device platform in this context and already form the basis of promising quantum cascade (QC) lasers[1] and QW photodetectors[2–5] at FIR wavelengths. While existing devices are mostly based on GaAs/AlGaAs QWs, III-nitride semiconductors have also been recently identified as potential candidates for use in this spectral range mainly due to their large LO-phonon frequencies (e.g., over 22 THz in GaN versus about 9 THz in GaAs). As a result, III-nitride ISB devices can operate at THz frequencies that are fundamentally inaccessible to their As-based counterparts due to reststrahlen absorption. Furthermore, such large LO-phonon frequencies are attractive as they can in principle enable the development of THz ISB devices operating at room temperature,[6] unlike all existing solutions.

Thus far, the investigation of ISB transitions in III-nitride semiconductors has mostly focused on the near-infrared and fiber-optic-communication spectral regions, motivated by the very large conduction-band offsets of GaN/Al(Ga)N QWs that allow for record short transition wavelengths. Several III-nitride ISB optoelectronic devices, including all-optical switches,[7,8] electro-optic modulators,[9] optically pumped light emitters,[10,11] and photodetectors,[12,13] have been demonstrated at near-infrared wavelengths. In addition, the observation of sequential tunneling transport in GaN/AlGaN coupled QWs has recently been reported,[14] which is promising for the development of complex QC structures based on this materials system. On the other hand, experimental studies of FIR ISB transitions in III-nitride QWs have so far been scarce.[15] In this Letter, we report the demonstration of an AlGaN ISB photodetector with responsivity peaked at a photon energy of about 54 meV (i.e., 13 THz frequency, or 23 μm wavelength).

In typical quantum well infrared photodetectors (QWIPs) based on ISB transitions,[16] the incident light is absorbed via the excitation of electrons from the ground-state to the first-excited subbands of several identical *n*-doped QWs grown on top of one another. A photocurrent is then created under an externally applied voltage bias, through the subsequent escape of the photoexcited electrons from the QWs into the continuum of unbound states over the barriers. The key design requirements are therefore a large oscillator strength of the absorbing transitions (which favors the use of well confined upper subbands) and efficient photoelectron escape out of the QWs (which favors the use of absorbing transitions directly into the continuum). In practice, the optimal tradeoff between these two conflicting requirements is often obtained with QWs where the first-excited subbands are nearly resonant with the conduction-band edge in the barriers,[16] leading to what are commonly referred to as bound-to-quasi-bound absorbing transitions.

While III-nitride near-infrared QWIPs have already been demonstrated,[12] the development of similar devices operating at FIR wavelengths is particularly complicated by the large internal electric fields that exist in these heterostructures due to their spontaneous and piezoelectric polarizations. To illustrate, in Fig. 1(a), we plot the conduction-band lineup and squared envelope functions of a GaN/AlGaN multiple-QW structure under bias, designed to provide ISB absorption between the lowest two subbands at a representative FIR photon energy of about 50 meV. These calculations were performed using a Schrödinger-equation solver that takes into account both pyro- and piezoelectric polarization fields assuming periodic boundary conditions, with all the relevant material parameters taken from Ref. 17. To obtain such a relatively small ISB transition energy in Fig. 1(a), a large well width [i.e., 57 monolayers (MLs), where 1 ML ≈ 2.6 Å] is used, which causes both ground-state and first-excited subbands to fall within the triangular portion of the QW potential energy profile. As a result, even though barriers with very small Al content (8%) are used, the first-excited subbands necessarily remain well below the onset of the barriers continuum, which limits the escape efficiency. Furthermore, the envelope-function spatial overlap

a)Electronic mail: rpaiella@bu.edu.

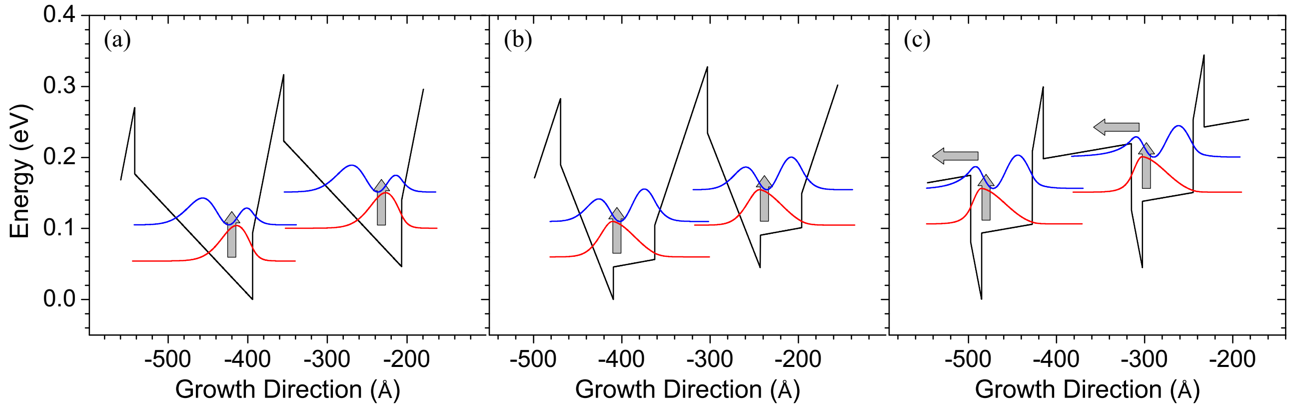

FIG. 1. Conduction-band lineups of three different AlGaN FIR QWIP structures under bias, where each repeat unit consists of: (a) a single $Al_{0.08}Ga_{0.92}N$ barrier and a single GaN well; (b) a single $Al_{0.08}Ga_{0.92}N$ barrier and a GaN/$Al_{0.04}Ga_{0.96}N$ step well; (c) a step $Al_{0.16}Ga_{0.84}N$/$Al_{0.08}Ga_{0.92}N$ barrier and a step GaN/$Al_{0.08}Ga_{0.92}N$ well. The squared envelope functions of the ground-state and first-excited subbands of each well are also shown, referenced to their respective energy levels. The vertical and horizontal arrows indicate, respectively, photon absorption and photoelectron escape into the continuum of unbound states over the barriers.

(and therefore the oscillator strength) between the bottom two subbands is somewhat degraded. A nearly flat potential energy profile can be established in the wells using the step-well design recently developed by Machhadani *et al.* to demonstrate THz ISB absorption in III-nitride QWs.[15] An exemplary QWIP based on this idea is shown in Fig. 1(b), where each well consists of two layers of different compositions (GaN and $Al_{0.04}Ga_{0.96}N$) and the bottom two subbands are again separated in energy by about 50 meV. With this approach, however, a large internal electric field still exists in the QW barriers, which again precludes the design of bound-to-quasi-bound QWIP structures.

In the present work, we propose the use of two different (Al)GaN compositions *both* in the wells and in the barriers in order to overcome the design limitations just described. By suitably choosing these compositions, one can create a multiple-QW potential energy profile where the effect of the internal electric fields is virtually eliminated, except for small energy "spikes" at the well-barrier interfaces. The first excited subbands can then be positioned at any desired energy relative to the top of the barriers, just like in the case of As-based devices. As an illustration, in Fig. 1(c), we plot the conduction-band diagram of the specific device developed in this work, where the fundamental ISB transition energy is computed to be 49 meV. In this structure, each step well consists of 5 MLs of GaN and 22 MLs of $Al_{0.08}Ga_{0.92}N$, while 5 MLs of $Al_{0.16}Ga_{0.84}N$ and 38 MLs of $Al_{0.08}Ga_{0.92}N$ are used in each step barrier. The first-excited subbands are relatively well confined within their respective QWs, while at the same time being energetically close to the overlaying continuum, as required for optimal QWIP performance.

Twenty repetitions of this double-step QW structure (beginning and ending with the 38-ML-thick $Al_{0.08}Ga_{0.92}N$ barrier layer) were grown on a 1×1 cm^2 substrate of commercially available free-standing GaN using rf plasma-assisted molecular beam epitaxy (MBE). Prior to this growth, the Al concentration versus flux was carefully calibrated using a similar substrate. In the grown sample, the multiple-QW active layer is embedded between a GaN template layer and a 200-nm-thick $Al_{0.08}Ga_{0.92}N$ cap layer, both of which are *n*-doped with Si to the level of 1×10^{18} cm^{-3}. With this choice of template and cap compositions, no significant voltage drop due to the intrinsic polarization fields is introduced across the multiple-QW layer, as confirmed by simulations of the entire conduction-band lineup based on commercial software (NextNano[3]). To enable strong ISB absorption between the ground-state and first-excited subbands, the 5-ML-thick GaN layer in each well is *n*-doped at a nominal concentration of 6×10^{18} cm^{-3}. In comparison, unintentional doping due to oxygen incorporation is expected to be significantly smaller under the MBE growth conditions employed in this work.[18] The sample periodicity was investigated via x-ray diffraction measurements, where clear superlattice satellite peaks could be resolved from which the repeat-unit thickness and average composition could be inferred. The calculated conduction-band diagram of Fig. 1(c) is based on these extrapolated values, which are close to their original targets.

After sample growth, 450×400 μm^2 mesa-structure devices were fabricated using standard photolithography and inductively coupled plasma etching (to a depth of approximately 730 nm) in a chlorine-based chemistry. Metal contacts consisting of a Ti/Al/Ti/Au multilayer structure were then deposited on top of and around each mesa. Contact resistivities on the order of a few 10^{-4} Ω-cm^2 were correspondingly measured after annealing at 850 °C for 50 s. The top contacts were also patterned in the shape of gratings with 9- or 12-μm period. In the photocurrent measurements described below, these gratings are used to couple normally incident light into the QWs in a way consistent with the polarization selection rules of ISB transitions. Incidentally, it should be noted that the GaN growth substrate is opaque at FIR wavelengths due to its relatively high background *n*-doping; as a result, polarization-resolved transmission and photocurrent measurements with the input light coupled through an angled facet lapped through the substrate could not be carried out with these samples. After metallization, the samples were annealed in a forming gas environment in order to passivate possible defects on the mesa sidewalls that could otherwise provide leakage current paths.

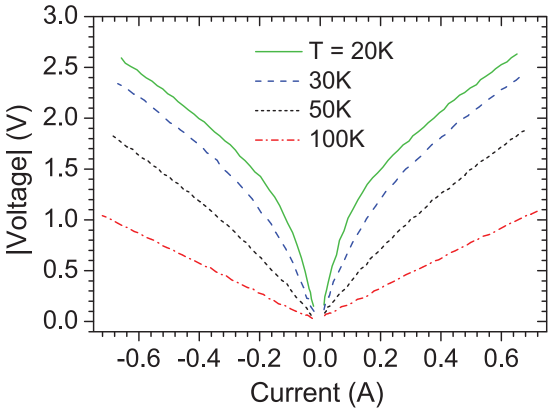

FIG. 2. Temperature-dependent dark I-V characteristics of a double-step AlGaN FIR QWIP developed in this work.

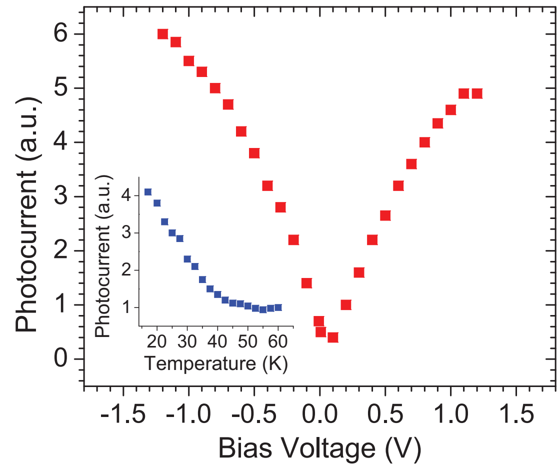

FIG. 3. Photocurrent signal of a double-step AlGaN FIR QWIP at a heat-sink temperature of 20 K versus applied voltage. Inset: photocurrent of the same device measured with a fixed bias of −0.6 V at different temperatures.

For electrical and optical characterization, the devices were finally soldered on a copper block with indium, wire-bonded to gold-coated ceramic platelletes, and mounted on the cold finger of a continuous-flow liquid-helium cryostat. In Fig. 2, we show the dark current-voltage (I-V) characteristics of one of these devices at different heat-sink temperatures measured with forward (i.e., positive from top to bottom) and reverse voltage pulses. At 100 K and above, the device is found to be highly conductive with nearly linear I-V characteristics, indicating very efficient thermal escape of electrons from the QWs. In contrast, as the temperature is lowered, the electrons in the wells become more tightly distributed near the bottom of the ground-state subbands, and tunneling into the adjacent continuum becomes the more important transport mechanism. Since the tunneling barrier is effectively lowered by the externally applied voltage, the I-V curves become strongly non-linear with sharper and sharper turn-on as the temperature is decreased. Electrical leakage paths due to structural defects in the active material may further contribute to the measured dark current, which may also explain the observation of similar I-V characteristics under both forward and reverse bias.

The device photocurrent spectra were measured using a Bruker IFS 66s Fourier transform infrared spectrometer (FTIR) with step-scan phase modulation and lock-in detection. In these measurements, light from the FTIR globar internal source is transmitted through the interferometer and then focused onto the device top surface with a paraboloidal Au-coated mirror. A bias tee is used to supply a DC voltage to the QWIP and to isolate the modulated photocurrent signal, which is detected with a combination of transimpedance and lock-in amplifiers and then fed back into the FTIR for spectral analysis. In Fig. 3, we plot the total photocurrent signal of a representative device with 9-μm grating period measured at 20 K as a function of applied DC bias. As the voltage is increased in either forward or reverse direction, the first-excited state of each QW becomes more and more strongly coupled to the adjacent barrier continuum, leading to an increase in photoelectron extraction efficiency and therefore in photocurrent. At the same time, the oscillator strength of the absorbing transitions decreases due to the reduced confinement of the upper states, and as a result, the photocurrent eventually saturates as the bias voltage is further increased. This saturation occurs at different values in the forward and reverse directions due to the slight asymmetry of the QW conduction-band lineup. As shown in the inset of Fig. 3, the measured photocurrent signal also decreases with increasing device temperature, due to increased thermal escape from the QWs, until it can no longer be resolved above the noise floor at about 50 K (where the I-V characteristics also become predominantly linear).

The photocurrent spectrum of the same device at 20 K under an applied bias of + 0.8 V is shown in Fig. 4 (solid line). Similar spectra were also obtained with 12-μm grating-period devices, albeit with smaller signal-to-noise ratio. The spectral response of the FTIR setup used in these measurements extends from about 13 to 82 meV (full width at half maximum), so that the shape of this trace fully reflects the device responsivity spectrum. The sharp cutoff on the short-wavelength side of the measured peak is due to the onset of the reststrahlen band of GaN (ranging from $h\nu_{TO} \approx 69$ meV to $h\nu_{LO} \approx 92$ meV, as indicated by the grey band near the horizontal axis), while the dips observed near the peak are caused by atmospheric absorption. A Gaussian theoretical fit to the

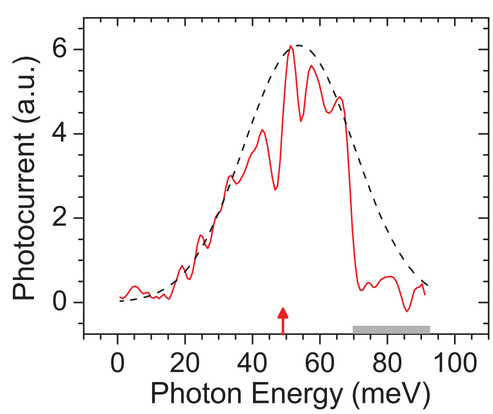

FIG. 4. Photocurrent spectrum of a double-step AlGaN FIR QWIP measured at 20 K under an applied voltage bias of +0.8 V (solid line), and Gaussian fit (dashed line). The grey band near the horizontal axis indicates the reststrahlen band of GaN. The vertical arrow indicates the calculated transition energy.

measured data (with these extraneous features removed) is shown by the dashed line in Fig. 4, whose peak photon energy of 54 meV is in good agreement with the calculated ISB transition energy of 49 meV (indicated by the vertical arrow). The difference can be mainly ascribed to thickness fluctuations in the experimental sample, where the narrower wells (absorbing at shorter wavelengths) can be expected to give a larger contribution to the overall photocurrent spectrum due to their larger photoelectron extraction efficiency.

Finally, the same photocurrent spectral measurements were carried out under identical conditions with a calibrated Gentec THZ9B-MT pyroelectric detector of known responsivity. By comparing the results of these measurements with the data obtained with the III-nitride QWIP of Figs. 3 and 4, we could estimate the responsivity of the latter device at 20 K to be approximately 7 mA/W. In previously demonstrated GaAs/AlGaAs FIR QWIPs (operating at longer THz wavelengths), responsivities ranging from about 10 mA/W to a few hundred mA/W were reported.[2–5] The relatively low value measured in our devices is mainly attributed to their large spectral linewidth (see Fig. 4), related to structural imperfections. In any case, the results presented in this work already indicate that double-step III-nitride QWs are promising for the development of FIR detectors that can extend the spectral coverage of As-based QWIPs, while retaining all the intrinsic advantages of ISB devices in general (i.e., great design flexibility, compact dimensions, suitability to monolithic integration, and high-speed response). The same design strategy can also be applied to the development of other FIR ISB devices based on III-nitride semiconductors, including modulators and QC light emitters.

This work was supported by the National Science Foundation under Grant No. ECS-0824116.

[1]B. S. Williams, Nature Photon. **1**, 517 (2007).

[2]A. G. U. Perera, S. G. Matsik, H. C. Liu, M. Gao, M. Buchanan, W. J. Schaff, and W. Yeo, Appl. Phys. Lett. **77**, 741 (2000).

[3]M. Graf, G. Scalari, D. Hofstetter, J. Faist, H. Beere, E. Linfield, D. Ritchie, and G. Davies, Appl. Phys. Lett. **84**, 475 (2004).

[4]H. Luo, H. C. Liu, C. Y. Song, and Z. R. Wasilewski, Appl. Phys. Lett. **86**, 231103 (2005).

[5]M. Patrashin and I. Hosako, Opt. Lett. **33**, 168 (2008).

[6]E. Bellotti, K. Driscoll, T. D. Moustakas, and R. Paiella, Appl. Phys. Lett. **92**, 101112 (2008).

[7]N. Iizuka, K. Kaneko, and N. Suzuki, IEEE J. Quantum Electron. **42**, 765 (2006).

[8]Y. Li, A. Bhattacharyya, C. Thomidis, T. D. Moustakas, and R. Paiella, Opt. Express **15**, 5860 (2007).

[9]L. Nevou, N. Kheirodin, M. Tchernycheva, L. Meignien, P. Crozat, A. Lupu, E. Warde, F. H. Julien, G. Pozzovivo, S. Golka, G. Strasser, F. Guillot, E. Monroy, T. Remmele, and M. Albrecht, Appl. Phys. Lett. **90**, 223511 (2007).

[10]L. Nevou, M. Tchernycheva, F. H. Julien, F. Guillot, and E. Monroy, Appl. Phys. Lett. **90**, 121106 (2007).

[11]K. Driscoll, Y. Liao, A. Bhattacharyya, L. Zhou, D. J. Smith, T. D. Moustakas, and R. Paiella, Appl. Phys. Lett. **94**, 081120 (2009).

[12]E. Baumann, F. R. Giorgetta, D. Hofstetter, H. Lu, X. Chen, W. J. Schaff, L. F. Eastman, S. Golka, W. Schrenk, and G. Strasser, Appl. Phys. Lett. **87**, 191102 (2005).

[13]A. Vardi, G. Bahir, F. Guillot, C. Bougerol, E. Monroy, S. E. Schacham, M. Tchernycheva, and F. H. Julien, Appl. Phys. Lett. **92**, 011112 (2008).

[14]F. Sudradjat, W. Zhang, K. Driscoll, Y. Liao, A. Bhattacharyya, C. Thomidis, L. Zhou, D. J. Smith, T. D. Moustakas, and R. Paiella, J. Appl. Phys. **108**, 103704 (2010).

[15]H. Machhadani, Y. Kotsar, S. Sakr, M. Tchernycheva, R. Colombelli, J. Mangeney, E. Bellet-Amalric, E. Sarigiannidou, E. Monroy, and F. H. Julien, Appl. Phys. Lett. **97**, 191101 (2010).

[16]B. F. Levine, J. Appl. Phys. **74**, R1 (1993).

[17]I. Vurgaftman and J. R. Meyer, J. Appl. Phys. **94**, 3675 (2003).

[18]T. D. Moustakas and A. Bhattacharyya, Phys. Status Solidi C **9**, 580 (2012).